Differential functions of the dorsal and intermediate regions of the hippocampus for optimal goal-directed navigation in VR space

Hyeri Hwang[1], Seung-Woo Jin[2], Inah Lee[1]*

[1]Department of Brain and Cognitive Sciences
Seoul National University
Gwanak-ro 1, Gwanak-gu
Seoul, Korea
08826

[2]Department of Psychiatry and Behavioral Sciences
University of Washington
1959 N.E. Pacific St, Seattle
WA, 98195, USA

*Corresponding author:
E-mail: inahlee@snu.ac.kr
Phone: +82-2-880-8013

Abstract

Goal-directed navigation requires the hippocampus to process spatial information in a value-dependent manner, but its underlying mechanism needs to be better understood. Here, we investigated whether the dorsal (dHP) and intermediate (iHP) regions of the hippocampus differentially function in processing place and its associated value information. Rats were trained in a place-preference task involving reward zones with different values in a visually rich VR environment where two-dimensional navigation was possible. Rats learned to use distal visual scenes effectively to navigate to the reward zone associated with a higher reward. Inactivation of the dHP or iHP with muscimol altered navigational patterns differentially. Specifically, measurements of the efficiency and accuracy of wayfinding behavior using directional analysis showed that iHP inactivation induced more severe damage to value-dependent navigation than dHP inactivation. Our findings suggest that the dHP is more critical for accurate spatial navigation to the target location per se, whereas the iHP is critical for finding higher-value goal locations.

Introduction

It has long been suggested that the hippocampus is the neural substrate of a 'cognitive map' – a map-like representation of the spatial environment that allows flexible spatial navigation (O'Keefe and Nadel, 1978). The cognitive map is also needed for remembering important events in space. Animals in the natural environment often navigate to achieve goals, such as finding food or avoiding predators, and this goal-directed navigation involves remembering places and their associated values. It has been reported that the receptive fields of place cells in the hippocampus tend to accumulate near a goal location or shift towards it (Hollup et al., 2001; Kennedy and Shapiro, 2009; Dupret et al., 2010). One could argue that the hippocampus must process task- or goal-relevant information, including the value of a place, to achieve the goal. However, the specific hippocampal processes involved in integrating the two types of representation – place and value – towards goal-oriented behavior are still largely unknown.

Such integration may occur along the dorsoventral axis of the hippocampus. Previous anatomical studies (Krettek and Price, 1977; Swanson et al., 1978; Pikkarainen et al., 1999; Tao et al., 2021) suggest that the hippocampus can be divided along its dorsoventral axis into dorsal (dHP), intermediate (iHP), and ventral (vHP) hippocampal subregions based on different anatomical characteristics. The dHP is connected with brain regions that process visuospatial information, including the retrosplenial cortex and the caudomedial entorhinal cortex (van Groen and Wyss, 2003; Dolorfo and Amaral, 1998); it also communicates with the iHP via bidirectional extrinsic connections but exhibits limited connections with the vHP (Tao et al., 2021; Swanson et al., 1978). The iHP receives heavy projections from valence-related areas, such as the amygdala and ventral tegmental area (VTA) – subcortical inputs that are less prominent in the dHP (Pikkarainen et al., 1999; Felix-Ortiz and Tye, 2014; Gasbarri et al., 1994). The vHP also has connections with the iHP and value-representing areas like the amygdala, but it does not project heavily to the dHP (Tao et al., 2021; Swanson et al., 1978; Pikkarainen et al., 1999; Krettek and Price, 1977). Notably, compared with the dHP, the iHP and vHP have much heavier connections with the medial prefrontal cortex (mPFC), contributing to goal-directed action control (Hoover and Vertes, 2007; Liu and

Carter, 2018). Additionally, the three subregions along the dorsoventral axis display different gene expression patterns that corroborate the anatomical delineations (Dong et al., 2009; Bienkowski et al., 2018). Overall, the iHP subregion of the hippocampus appears to be ideally suited to integrating information from the dHP and vHP.

Surprisingly, beyond the recognition of anatomical divisions, little is known about the functional differentiation of subregions along the dorsoventral axis of the hippocampus. Moreover, the available literature on the subject is somewhat inconsistent. Specifically, there is physiological evidence that the size of a place field becomes larger as recordings of place cells move from the dHP to the vHP (Jung et al., 1994; Kjelstrup et al., 2008; Royer et al., 2010). Thus, it has been thought that the dHP is more specialized for precise spatial representation than the iHP and vHP. However, when it comes to the neural representation of value information of a place, results are mixed. Several studies have reported that place fields recorded in the dHP respond to internal states and motivational significance based on their accumulation near behaviorally significant locations (e.g., reward locations or escape platforms; Hollup et al., 2001; Kennedy and Shapiro, 2009; Dupret et al., 2010), or to the reward per se (Gauthier and Tank, 2018). In contrast, others have reported that dHP place cells do not alter their activity according to a change in reward or reward location and thus do not represent value information (Duvelle et al., 2019; Jin and Lee, 2021; Speakman and O'Keefe, 1990).

Furthermore, although the iHP and vHP have mainly been studied in the context of fear and anxiety, several studies have also reported spatial representation and value-related signals in these subregions. Specifically, prior studies reported that rats with a dysfunctional dHP retained normal goal-directed, target-searching behavior if the iHP and vHP were intact (Moser et al., 1995; de Hoz et al., 2003). Moreover, lesions in the iHP have been shown to impair rapid place learning in the water maze task (Bast et al., 2009). Our laboratory also reported that place cells in the iHP, but not the dHP, instantly respond to a change in spatial value and overrepresent high-value locations (Jin and Lee, 2021).

Based on existing experimental evidence, we hypothesize that the iHP is the primary locus for associating spatial representation with value information, distinguishing it from the dHP and vHP. In the current study, we investigated the differential functions of the dHP and

iHP in goal-directed spatial navigation by monitoring behavioral changes after pharmacological inactivation of either of the two regions as rats performed a place-preference task in a two-dimensional (2D) virtual reality (VR) environment. In this experimental paradigm, rats learned to navigate toward one of two hidden goal locations associated with different reward amounts. Whereas inactivation of the dHP mainly affected the precision of wayfinding, iHP inactivation impaired value-dependent navigation itself.

Results

Well-trained rats align themselves toward the high-value zone before departure in the place-preference task

We established a VR version of a place-preference task (**Figure 1A**) in which rats could navigate a 2D environment by rolling a spherical treadmill with their body locations fixed, allowing them to run at the apex of the treadmill. Body-fixed rats (n = 8) were trained to explore a virtual circular arena surrounded by multiple distal visual landmarks (houses, rocks, mountains, and trees) (**Figure 1B**). Rats were always started at the center of the arena, and the arena contained two unmarked reward zones – a high-value zone and a low-value zone – each associated with different amounts of honey water (6:1 ratio between high- and low-value zones). A trial started with the rat facing one of six start directions – north (N), northeast (NE), southeast (SE), south (S), southwest (SW), and northwest (NW) – determined pseudorandomly to guarantee equal numbers of trials in all directions. In the example trial shown in **Figure 1C**, the rat was heading in the NE direction at the start location ('Trial Start'), then turned to the left side to run toward the W goal zone ('Navigation'). Once the rat arrived at one of the reward zones, the synchronization between the spherical treadmill movement and the virtual environment stopped, and multiple drops of honey water were delivered via the licking port ('Reward'). Then, during an inter-trial interval (ITI), the LCD screens turned gray, and the rat was required to remain still for 5 seconds to initiate the subsequent trial. The pre-surgical training session consisted of 60 trials, which were reduced

142 to 40 during post-surgical training.

143 Pre-surgical training began after shaping in the VR environment. On average, it took
144 13 days for rats to reach pre-surgical criteria, namely, to complete 60 trials and visit the high-
145 value goal zone in more than 75% of completed trials (see Methods for the detailed
146 performance criteria). Well-trained rats exhibited two common behaviors during the pre-
147 surgical training. First, they learned to rotate the spherical treadmill counterclockwise to
148 move around in the virtual environment (presumably to perform energy-efficient navigation).
149 Second, once a trial started, but before leaving the starting point at the center, the animal
150 rotated the treadmill to turn the virtual environment immediately to align its starting direction
151 with the visual scene associated with the high-value reward zone. After setting the starting
152 direction, the rat started to run on the spherical treadmill, moving the treadmill forward to
153 navigate directly toward the reward zone. All eight rats displayed this strategy during the
154 later learning phase but not during the earlier learning stage, suggesting that the start-scene–
155 alignment strategy was learned during training. Because the initial rotational scene alignment
156 before departure was an essential component of the task and this behavior was not readily
157 detectable with position-based analysis, we based most of our behavioral analysis on the
158 directional information defined by the allocentric reference frame of the virtual environment
159 (**Figure 2A**). Because we did not measure the rat's head direction in the current study, the
160 allocentric directional information represented the angular position of a particular scene in the
161 virtual environment displayed in the center of the screen.

162 To establish the direction in which the rat departed the starting point at the center
163 after scene alignment, we first defined a *departure circle* – a virtual circle (~20 cm in
164 diameter) in the VR environment at the center of the arena (**Figure 2A**). In the example trial
165 shown in **Figure 2A**, the rat faced the NE direction (315°) at the trial start but immediately
166 turned its body to the NW direction upon starting and ran straight toward the high-value zone
167 after that. Since the initial scene rotations at the start point cannot be visualized in the
168 position-based graph, we made a *scene rotation plot* that visualizes the rotational movement
169 traces in the virtual environment. The scene rotation plot covers the period from the start of
170 the trial to when the rat leaves the starting point at the center and the departure circle (**Figure**
171 **2B**).

172 On the first day of training for the task ('Novice' stage), the rat produced almost no
173 rotation of the VR environment until he exited the departure circle, indicating that the animal
174 ran straight in the initially set start direction without adjusting the scene orientation. As a
175 result, rats missed the target reward zones in most trials (**Figure 2B** and **2C**). However, by
176 the last day of training ('Expert' stage), there were noticeable rotational shifts in all
177 directional traces (i.e., counterclockwise rotations) that converged on the high-value reward
178 zone (**Figure 2B** and **2D**). This was the case for all trials except those in which the initial
179 start direction almost matched the orientation of the high-value reward zone (i.e., 225° or
180 NW). Furthermore, the average travel distance and latency for each start direction declined
181 from the novice to the expert stage, suggesting that the rats navigated more efficiently toward
182 reward zones in the later stage of learning by pre-adjusting their starting scene direction at the
183 trial start (**Figure 2C** and **2D**).

184 Overall, the marked differences in orienting behaviors between early and late
185 learning stages suggest that rats could discriminate the high-value reward zone from the low-
186 value zone in our VR environment and show that they preferred visiting the high-value
187 reward zone over the low-value zone. It also indicates that rats could explore the VR
188 environment using allocentric visual cues to find the critical scenes associated with the high-
189 value zone before leaving the starting point (i.e., departure circle).

190

191 **Departing orientation and perimeter-crossing direction provide a measure of**
192 **navigational efficiency and accuracy, respectively**

193 To analyze behavioral changes during learning in more detail, we analyzed various learning-
194 related parameters at different stages of pre-surgical training. For this, we focused on days in
195 which rats visited the high-value zone on more than 75% of trials for two consecutive days –
196 the performance criterion for completion of pre-surgical training. These two consecutive days
197 (post-learning days) were grouped and averaged for each rat as the post-learning group
198 ('POST' in **Figure 3A-ii**) and compared with the two consecutive days immediately
199 preceding the post-learning days (pre-learning days; 'PRE' in **Figure 3A-ii**).

200 We first measured the departing direction when crossing the departure circle

(Departing Direction [DD]; **Figure 3A-i**). As indicated in **Figure 2**, well-trained rats rotated the VR environment to place the target VR scene (i.e., high-value reward zone scene) ahead before departure. Therefore, alignment of the departure direction with the high-value zone at the beginning of navigation indicated that the rat remembered the scenes associated with the high-value zone. For example, the distribution of pre-learning days departure directions was widely distributed without any directional bias; as such, its mean vector was small (**Figure 3A-ii**). On the other hand, the departure directions of post-learning sessions mostly converged on the direction aligned with the high-value zone, resulting in a larger mean vector length compared with that in the pre-learning session. The distributions of averaged departure directions for all rats significantly differed between 'PRE' and 'POST' ($p < 0.001$, Kuiper's test), verifying that departure direction is a valid index of the acquisition of the high-value zone and efficient navigation. To investigate how accurately rats oriented themselves directly to the high-value zone before leaving the start point, we also calculated the average deviation angle of departure directions (DD-deviation) – the angle between the departure direction and the high-value zone (180°, measured at the center of the zone) – for each rat (**Figure 3A-iii**). A comparison between pre- and post-learning sessions showed that the DD-deviation significantly declined after learning. This implies that well-learned rats aligned their bodies more efficiently to directly navigate to the high-value zone ($p < 0.01$, Wilcoxon signed-rank test).

Rats adjusted their navigational routes further, even after exiting the departure circle, to navigate more accurately and straight to the goal, avoiding the wall surrounding the arena. Such fine spatial tuning (i.e., navigation accuracy), measured as the decrease in DD-deviation, only appeared after the rats learned the high-value reward location. To quantify navigation accuracy, we measured the perimeter-crossing direction (PCD; **Figure 3B-i**), defined as the angle at which the rat first touched the unmarked circular boundary along the arena's perimeter, which shares the inner boundaries of the reward zones (green dashed lines in **Figure 3B-i**). During pre-learning, the PCD was randomly distributed along the perimeter ('PRE' in **Figure 3B-ii**). On the other hand, in most post-learning stage trials, rats crossed the unmarked peripheral boundaries only in the vicinity of the high-value zone ('POST' in **Figure 3B-ii**). Since rats usually turned counterclockwise during navigation, the convergence of crossings near the northern edge of the high-value zone indicates that they took a shortcut

– the most efficient route – to enter the goal zone. The PCD distributions were significantly different between pre- and post-learning stages ($p < 0.001$; Kuiper's test) (**Figure 3B-ii**). The deviation angle between the PCD and the high-value zone center also significantly decreased with learning (**Figure 3B-iii**), indicating that the navigation of rats to the goal became more accurate.

Navigation is impaired by inactivation of either the dHP or iHP, but only iHP inactivation affects place-preference behavior

To dissociate the roles of the dHP and iHP, we inactivated either the dHP or iHP in an individual animal using muscimol (MUS), a GABA-A receptor agonist, before the rat performed the place-preference task. To allow within-subject comparisons in performance, we bilaterally implanted two pairs of cannulas – one targeting the dHP and the other targeting the iHP – in the same rat after it successfully reached pre-surgical training criteria (**Figure 4A**). After 1 week of recovery from surgery, rats were retrained to regain a level of performance similar to that in the pre-surgical training period (**Figure 4B**), after which the drug injection schedule was started.

We divided rats into two drug-injection groups (n = 4 rats/group) to counterbalance the injection order between the dHP and iHP. Rats in one group received drug infusion into the dHP first, whereas rats in the other group were injected into the iHP first. For all rats, phosphate-buffered saline (PBS) was initially injected in both regions as a vehicle control. For analytical purposes, we first ensured no statistical difference in performance between the two PBS sessions (dPBS and iPBS; see below) and then averaged them into a single PBS session to increase statistical power. During the PBS session, rats tended to take the most efficient path to the high-value zone, as they had done during pre-surgical training (**Figure 5A**). They aligned the VR scene at the start with the high-value zone for all start directions and then ran directly toward the goal zone. Notably, once the start scene alignment was complete, rats usually moved quickly and straight without slowing in the middle. Also, their navigation paths led them directly toward the center of the goal zone. During subsequent dHP-inactivation sessions, rats appeared less accurate, bumping into the arena wall in many trials (dMUS in **Figure 5A**), but most of these wall bumps occurred in the vicinity of the

262 high-value zone, and rats quickly compensated for their error by turning their bodies to target
263 the reward zone correctly after wall bumping. In contrast, in iHP-inactivation sessions, the
264 trajectories were largely disorganized, and the wall-bumping locations were no longer limited
265 to the vicinity of the high-value zone. In some trials, rats moved largely randomly (as shown
266 in 860-17-24 in **Figure 5A)** and appeared to visit the low-value zone significantly more than
267 during PBS or dMUS sessions.

268 To quantitatively analyze these observations, we compared the proportions of visits
269 to the high-value zone among drug conditions (**Figure 5B**), finding a significant difference in
270 the percentage of correct target visits among drug conditions ($F_{(2,14)} = 10.56$, $p < 0.01$, one-
271 way repeated-measures ANOVA; $p = 0.25$ for dPBS vs. iPBS, Wilcoxon signed-rank test). A
272 post hoc analysis revealed a significant decrease in the iMUS session compared to the PBS
273 session ($p < 0.05$, Bonferroni-corrected post hoc test). In contrast, no significant differences
274 were found in other conditions, although there was a decreasing trend in the iMUS compared
275 to PBS ($p = 0.2$ for PBS vs. dMUS; $p = 0.1$ in dMUS vs. iMUS). These results indicate that
276 dHP-inactivated rats show a strong preference for the high-value zone, as they did in control
277 sessions, but that the performance of iHP-inactivated rats was impaired in our place-
278 preference task, as reflected in their significantly more frequent visits to the low-value zone
279 compared with controls.

280 It is unlikely that these differences stemmed from generic sensorimotor impairment
281 as a result of MUS infusion because running speed remained unchanged across drug
282 conditions ($F_{(2,14)} = 0.99$, $p = 0.37$, one-way repeated-measures ANOVA; $p = 0.95$ for dPBS
283 vs. iPBS, Wilcoxon signed rank test) (**Figure 5C**). Furthermore, rats remained motivated
284 throughout the testing session, as evidenced by the absence of a significant difference in the
285 number of trials across drug groups ($F_{(1.16, 8.13)}=1.34$, $p = 0.29$, one-way repeated-measures
286 ANOVA with Greenhouse-Geisser correction; $p = 1.0$ for dPBS vs. iPBS, Wilcoxon signed
287 rank test; data not shown), although there was an increase in the session duration ($F_{(2,14)} =$
288 6.46, $p < 0.05$, one-way repeated-measures ANOVA; $p = 0.27$ for dPBS vs. iPBS, Wilcoxon
289 signed rank test; data not shown) during MUS sessions (dMUS and iMUS) compared with
290 the PBS session (p-values < 0.05, Bonferroni-corrected post hoc test). This increase in
291 session duration was attributable to arena wall bumping events, which usually entailed a
292 recovery period before rats left the peripheral boundaries and moved again toward the goal.

These observations indicate that inactivation of the iHP significantly impairs the rat's ability to effectively navigate to the higher-value reward zone in a VR environment without affecting goal-directedness or locomotor activity.

To determine how effectively rats traveled to the goal in each condition, we also quantified the errors made in each condition by assessing the number of perimeter crossings (**Figure 5D**). To avoid duplicate assessments, we only counted an event as a perimeter crossing when the rat crossed the perimeter boundary from inside to outside. Rats tended to make more errors in dMUS sessions compared with controls, and errors were even more prevalent in iMUS sessions ($F_{(2,14)} = 18.59$, $p < 0.001$, one-way repeated-measures ANOVA; $p = 0.39$ for dPBS vs. iPBS, Wilcoxon signed rank test; $p < 0.01$ for PBS vs. dMUS, $p < 0.01$ in PBS vs. iMUS; $p < 0.05$ for dMUS vs. iMUS, Bonferroni-corrected post hoc test). During PBS sessions, navigation was mostly precise, resulting in just one perimeter crossing. In the dMUS sessions, accuracy declined, but the rats were relatively successful in finding the high-value zone, with most trials being associated with a slightly increased number of perimeter crossings. In contrast, rats in the iMUS sessions failed to find the high-value zone. They seemed undirected, exhibiting a significantly increased number of perimeter crossings compared with the other two sessions. Taken together, these results indicate that iHP inactivation severely damages normal goal-directed navigational patterns in our place-preference task.

The dHP is important for navigational precision, whereas the iHP is necessary for value-dependent spatial navigation

To further differentiate among conditions, we examined departure direction and PCD – indices of the effectiveness and accuracy of navigation, respectively (**Figure 3**). We first investigated the distribution of departure directions in all trials for all rats and calculated the resultant mean vector (**Figure 6A**). Whereas departure directions for both PBS sessions (dPBS and iPBS) were distributed relatively narrowly towards the high-value zone, those for dMUS sessions were more widely distributed, and their peak pointed away from the reward zone. In the case of the iHP-inactivation session, some departure directions were even pointed towards the opposite side of the target goal zone (i.e., the low-value zone). Thus, the

323 mean vectors from PBS sessions were relatively longer than those from MUS sessions. The
324 mean vectors for PBS sessions also stayed within the range of the high-value zone, whereas
325 those for MUS sessions pointed either toward the edge of the reward zone (dMUS) or the
326 outside of the reward zone (iMUS).

327 We next quantitatively confirmed these observations, comparing the mean direction
328 for each drug condition to determine how inactivation affected the accuracy of the body
329 alignment of rats at departure (**Figure 6A**). A Watson-Williams test indicated that the mean
330 angles of departure directions in all four drug conditions (dPBS, iPBS, dMUS, and iMUS) for
331 all rats significantly differed from each other ($F_{(3,1253)} = 7.78$, $p < 0.001$). Post hoc pairwise
332 comparisons showed that inactivation of either the dHP or iHP significantly altered departure
333 directions compared with the PBS condition ($p < 0.05$ for dPBS vs. dMUS; $p < 0.001$ for
334 iPBS vs. iMUS; $p = 0.66$ for dPBS vs. iPBS; Watson-Williams test). Moreover, the mean
335 departure directions of dMUS and iMUS sessions were displaced from the center of the high-
336 value zone compared with those of PBS sessions (i.e., dPBS and iPBS), suggesting that the
337 rats did not accurately align themselves to the target reward zone at the time of departure.
338 The mean vector of the iMUS session also appeared smaller than that of the other conditions,
339 indicating a less concentrated distribution of departure directions with iHP inactivation.
340 Unfortunately, it was not possible to perform a statistical comparison between dMUS and
341 iMUS because the departure directions for the iMUS session were too dispersed to yield a
342 mean vector with a sufficient length to compare directions between the two conditions
343 (averaged mean vector length of dMUS and iMUS sessions < 0.45; Berens, 2009).

344 The mean vector lengths for departure directions were also significantly different
345 among drug conditions ($F_{(2,14)} = 12.64$, $p < 0.001$, one-way repeated-measures ANOVA; $p =$
346 0.55 for dPBS vs. iPBS, Wilcoxon signed rank test) (**Figure 6B**), with a post hoc analysis
347 showing a significant difference between the iMUS session and both PBS ($p < 0.01$) and
348 dMUS ($p = 0.05$) sessions; however, no significant difference was found between PBS and
349 dMUS sessions ($p = 0.24$, Bonferroni-corrected post hoc test). The profound performance
350 deficits in the iHP-inactivated condition were also confirmed by examining the DD-deviation
351 from the target direction, defined as the center of the high-value zone (**Figure 6C**).
352 Specifically, we found that DD-deviations were significantly different among drug conditions
353 ($F_{(2,14)} = 13.37$, $p < 0.001$, one-way repeated-measures ANOVA; $p = 0.38$ for dPBS vs. iPBS,

Wilcoxon signed-rank test), with a Bonferroni-corrected post hoc test revealing a significant increase in DD-deviation in the iMUS session compared with both the PBS session ($p < 0.01$) and the dMUS session ($p < 0.05$). Again, no significant difference was found between PBS and dMUS sessions ($p = 0.19$). These results demonstrate that disruption of the dHP does not significantly affect the ability of rats to orient themselves effectively at departure to target the high-value reward zone. In contrast, inactivation of the iHP across all trials caused rats to depart the starting location without strategically aligning to the scene and consequently failing to hit the target zone effectively and directly.

Next, we ran similar analyses for the PCD (**Figure 7**), also investigating the PCD distribution and its mean vector for each drug condition (**Figure 7A**). PCD distributions appeared similar to those for departure direction; the PCD distributions of PBS sessions were narrowly contained within the high-value reward zone, whereas those of MUS sessions were more dispersed and misaligned with the reward zone. Again, the PCD distribution of the iMUS session showed some occurrences near the low-value zone. An examination of the resulting mean vectors using a Watson-Williams test revealed a significant difference in mean PCD angle in all sessions except for the comparison between the two PBS sessions ($F_{(3,1253)} = 16.22$, $p < 0.001$; $p = 0.08$ for dPBS vs. iPBS). The mean PCD angle of the dMUS session was shifted toward the upper end of the high-value zone ($p < 0.001$ for dPBS vs. dMUS), whereas that of the iMUS session was outside of the reward zone ($p < 0.001$ for iPBS vs. iMUS). Notably, iHP inactivation resulted in more severe errors in finding the high-value zone than dHP inactivation ($p < 0.01$ for dMUS vs. iMUS). Interestingly, with iHP inactivation, several PCDs were found near the low-value zone, an outcome that rarely occurred in other conditions. Considering the decreased percentage of high-value zone visits (**Figure 5**), some of these trials ended with the rat visiting the low-value zone, suggesting an impaired ability of the animal to perform goal-directed navigation strategically.

The PCD mean vector length was largest in the PBS condition, shortest in the iMUS condition, and intermediate in the dMUS condition ($F_{(2,14)} = 15.67$, $p < 0.001$, one-way repeated-measures ANOVA; $p = 0.55$ for dPBS vs. iPBS, Wilcoxon signed rank test) (**Figure 7B**). Unlike the mean vector length for departure direction, the PCD mean vector length differed between PBS and dMUS sessions, suggesting that wayfinding behavior is explicitly disrupted by dHP inactivation, albeit to a lesser extent compared with iHP inactivation ($p <$

385 0.05 for PBS vs. dMUS; $p < 0.01$ for PBS vs. iMUS; $p = 0.06$ for dMUS vs. iMUS,
386 Bonferroni-corrected post hoc test).

387 On the other hand, the PCD deviation angle from the center of the high-value zone
388 increased in inverse order: smallest in the PBS condition and largest in the iMUS condition
389 ($F_{(2,14)} = 17.24$, $p < 0.001$, one-way repeated-measures ANOVA; $p = 0.55$ for dPBS vs. iPBS,
390 Wilcoxon signed rank test) (**Figure 7C**). Similar to the PCD mean vector length data, the
391 significant increase in deviation angle after dHP inactivation indicates that dHP-inactivated
392 rats failed to achieve fine spatial tuning toward the high-value zone compared with controls
393 ($p < 0.05$ for PBS vs. dMUS, Bonferroni-corrected post hoc test). iHP inactivation also
394 resulted in less accurate navigation, including perimeter crossings – effects that were more
395 severe than those caused by dHP inactivation ($p < 0.01$ for PBS vs. iMUS; $p = 0.06$ for
396 dMUS vs. iMUS, Bonferroni-corrected post hoc test).

397 Overall, results based on the PCD measure revealed that dHP-inactivated rats showed
398 decreased accuracy in arriving at the goal, as reflected in the significant deviation of their
399 PCD from the high-value zone. The PCD distribution was also not as narrow as under control
400 conditions. Notably, deficits in navigation performance were even more severe in rats with
401 iHP inactivation, and their performance impairment was qualitatively different from that
402 observed with dHP inactivation in terms of both efficiency and accuracy of navigation.
403 Again, these results suggest that, while the dHP is essential for accurate wayfinding, the iHP
404 is crucial for value-dependent navigation to the higher-reward location.

405

406 **Hippocampal inactivation does not impair cue-guided navigation or goal-directedness**

407 After the drug-injection stage, we trained five of the same rats used in the main task in a
408 visual cue-guided navigation task to verify whether MUS inactivation of the hippocampus
409 resulted in deficits in goal-directed navigation in general (**Figure 8A-i**). We used the same
410 circular arena from the main task but removed all allocentric visual landmarks. The rat was
411 started from a fixed location near the periphery of the arena. As the trial started, a spherical
412 visual landmark with a checkered pattern flickered on either the left or right side
413 (pseudorandomized across trials) of the rat's starting position, serving as a beacon. When the

rat arrived at the landmark area (see Methods), the connection between treadmill movement and the virtual environment stopped, and honey water was provided as a reward. The rewards provided by left and right reward zones were the same in terms of both quality and quantity.

In this version of the navigation task, the rat's navigation was simply guided by the visual beacon, a type of task that the literature suggests is not hippocampus-dependent (Morris et al., 1986; Packard et al., 1989). Rats learned the task rapidly. Specifically, it took 3 days on average for rats to reach the criterion of completing 40 trials with an excess travel distance of less than 0.1 meters (see Methods). Moreover, examining their trajectories suggested that rats had no problem moving toward the visual landmark, whether it appeared on the left or right of the starting location (**Figure 8A-ii**). Rats arrived at the reward zone directly in most trials ('Direct hit') but bumped into the arena wall in some trials. Given the presence of a strong visual landmark, which served as a beacon, trials in which the rat bumped the arena walls were considered failed trials (**Figure 8A-ii**).

Finally, we applied the same drug injection schedule for the main task after the rats reached the abovementioned criterion. A one-way repeated-measures ANOVA revealed that the proportion of direct-hit trials did not significantly differ across drug conditions, indicating no significant change in navigation accuracy when the goal was marked by the visual beacon ($F_{(2,8)} = 1.60$, $p = 0.26$; $p = 0.50$ for dPBS vs. iPBS, Wilcoxon signed rank test) (**Figure 8B**). These results also imply that no generic sensory-motor or motivational deficits were involved. Collectively, these observations confirm that MUS injections in the hippocampus do not alter the ability of the rat to move around freely in the VR environment in a goal-directed fashion when the hippocampus is not necessary for the task.

Discussion

In the current study, we inactivated the dorsal or intermediate hippocampal region in rats performing a place-preference task in VR space to investigate the functional differentiation along the dorsoventral hippocampal axis during goal-directed navigation. Inactivation of the

443 intermediate region, but not the dorsal region, of the hippocampus produced a marked
444 reduction in the rat's ability to conduct strategic goal-directed navigation in the virtual space
445 without affecting goal-directedness or locomotor ability. We further examined navigational
446 quality by measuring the accuracy of scene alignment upon departure and by assessing the
447 efficiency (i.e., directness) of travel to the target goal zone (i.e., higher-value zone) without
448 bumping into walls on the arena boundaries. We found that dHP-inactivated rats were
449 modestly, but significantly, impaired, not only in precisely targeting the goal at the time of
450 departure but also in effectively traveling to the goal zone, compared with controls.
451 Importantly, however, the ability of these dHP-inactivated rats to head toward the higher-
452 value zone in the VR environment was unimpaired. In contrast, iHP-inactivated rats were
453 severely impaired in the initial targeting of the goal zone at the time of departure and traveled
454 somewhat aimlessly in the VR environment compared with both controls and dHP-
455 inactivated rats. Our findings suggest that the dHP is essential for finding the most effective
456 travel path for precise spatial navigation and that the iHP is necessary for navigating the
457 space in a value-dependent manner to achieve goals.

458

459 **Rats use allocentric visual scenes and landmarks to target the goal zone and adjust their**
460 **paths accordingly during navigation in the VR environment**

461 In the current paradigm, rats rotated the spherical treadmill counterclockwise immediately
462 after the trial started at the VR arena's center, presumably to find the visual scene to guide
463 them directly toward the goal zone (i.e., high-value zone) upon departure. This initial
464 orientation of departure – or departure direction (DD) – seems critical in our task, as
465 evidenced by the fact that, during training, rats that miscalculated the departure direction
466 usually bumped into the wall and had to reorient themselves at various positions within the
467 environment. Once the rats learned the task, they oriented themselves before leaving the start
468 point by rotating the visual environment until they found the goal-associated visual scenes
469 and then ran straight toward the goal zone. These behavioral characteristics suggest that our
470 task is heavily dependent on the rat's ability to use the allocentric reference frame of the
471 visual environment.

472 Prior studies suggest that, in an environment where the directional information comes

473 largely from allocentric visual cues, the spiking activity of place cells is significantly
474 modulated by directional visual cues, a finding that holds in both real and virtual
475 environments (Acharya et al., 2016; Ravassard et al., 2013; Aronov and Tank, 2015). In one
476 of these studies (Acharya et al.), directional modulation of place cells was observed even
477 during random foraging in the absence of a goal-directed memory task. Notably, this was also
478 true for spatial view cells in nonhuman primates (Rolls and O'Mara, 1995; Georges-Francois
479 et al., 1999). Although we did not record place cells in our study, hippocampal place cells
480 could be predicted to exhibit directional firing patterns associated with the visual scenes
481 along the periphery of the current VR environment. Because rats in the current study rotated
482 the environment until they found the target-matching scene without leaving the center starting
483 point, our VR task may be an ideal behavioral paradigm for examining the directional firing
484 of place cells in future studies.

485

486 **Inactivating the dHP impairs navigational precision but does not affect place preference**
487 **based on differential reward values**

488 Our working model posits that the dHP represents a fine-scaled spatial map of an
489 environment, in this case, a VR environment, that allows an animal to map its location
490 precisely and choose the most efficient travel routes. Our experimental results support this
491 model, demonstrating that dHP-inactivated rats deviated slightly, but significantly, from the
492 ideal target heading at the time of departure (measured by departure direction), resulting in
493 crossing the area boundary near the target goal zone. Nonetheless, it is important to note that
494 dHP-inactivated rats in our study oriented themselves normally in the direction of the high-
495 value reward zone at the time of departure, suggesting that the value-coding cognitive map
496 and its use were intact and able to spatially guide the rats to the high-reward area in the
497 absence of a functioning dHP. We argue that such intact place preference performance with
498 reasonable spatial navigation ability is supported by the iHP (presumably in connection with
499 the vHP) in dHP-inactivated rats.

500 Whether the dHP represents value signals remains a matter of controversy.
501 According to previous studies, place fields of the dHP seem to translocate to or accumulate
502 near the location with motivational significance (e.g., reward zone), and where the strategic

503 importance is higher (e.g., choice point in the T-maze) (Hollup et al., 2001; Lee et al., 2006;
504 Kennedy and Shapiro, 2009; Dupret et al., 2010; Ainge et al., 2011; Valenti et al., 2018). For
505 instance, the overrepresentation of the escape platform in a water maze – a location of high
506 motivational significance – was observed in the neural firing patterns of place cells in the
507 hippocampus (Hollup et al., 2001). In addition, Lee et al. reported that dHP place fields
508 gradually translocate toward the goal arm of a continuous T-maze (Lee et al., 2006), and
509 Dupret and colleagues suggested a goal-directed reorganization of hippocampal place fields
510 based on an experimental paradigm in which reward locations were changed daily (Dupret et
511 al., 2010). Such accumulation of spatial firing is not restricted to the goal location, as place
512 fields recorded from the dHP were reported to be unevenly distributed near the start box and
513 the choice point of a T-maze (Ainge et al., 2011). One potential explanation for the
514 discrepancy between our study and studies that reported apparent valence-dependent signals
515 in the dHP could be that the dHP processes motivational and strategic significance (from the
516 perspective of task demand), which is not always the same as the reward. Significance might
517 include task demand, such as a change between random and directed search of reward
518 (Markus et al., 1995), or a change in a significant environment stimulus from which the goal
519 location needs to be calculated (Gothard et al., 1996). However, none of these were changed
520 in our experimental paradigm, which might explain why dHP inactivation did not affect
521 place-preference behavior.

522 Another possibility is that the dHP responds only to a more radical change in value,
523 such as the presence or absence of reward, but not to different amounts of the same reward.
524 Indeed, hippocampal neuronal activity does not show an explicit response to reward value in
525 rats trained to visit arms of a plus-maze in descending order of reward amount (Tabuchi et al.,
526 2002). Moreover, when the reward is unexpectedly altered to a less preferred one, thus
527 decreasing motivational significance, place cells in the dHP remain mostly unchanged (Jin
528 and Lee, 2021). These results suggest that the dHP is not crucial to maintaining value
529 preference, a finding in line with the observed absence of an effect on place preference after
530 dHP inactivation in our study. A recent study in which mice were trained to associate a
531 particular odor with an appetitive outcome and distinguish it from the non-rewarded odor
532 suggested that the dHP is responsible for stimulus identity, not saliency (Biane et al., 2023).
533 This might be another possible interpretation of our dHP results since we used the same

honey water reward for both reward zones.

The iHP may contain a value-associated cognitive map with reasonable spatial resolution for goal-directed navigation

iHP-inactivated rats showed poor goal-directed navigation, characterized by misalignment of their departing orientation with the goal zone and arrival points that were often far removed from the goal zone compared with the same rats under both control and dHP-inactivated conditions. These results support our working model that the iHP is critical for representing a value-associated cognitive map of the environment. iHP-inactivated rats, presumably unable to utilize such a value-representing map, could not strategically plan and organize their behaviors to target the high-value area in the current study. Consequently, the precise spatial map present in the dHP may be of little use without the guidance of the value-associated map in the iHP, accounting for the poor navigational performance of iHP-inactivated rats. The value-associated cognitive map in the iHP may still show reasonable spatial specificity, as evidenced by the larger, but still specifically located, place fields in the iHP compared with the dHP (Jin and Lee, 2021).

The involvement of the iHP in spatial value association has been reported in several studies. For example, Bast and colleagues reported that rapid place learning is disrupted by removing the iHP and vHP, even when the dHP remains undamaged (Bast et al., 2009). On the other hand, if the iHP is spared but the dHP and vHP are removed by lesioning, rats in a water maze test quickly learn a new platform location normally. Moreover, a change in reward value induced an immediate global remapping response and a greater overrepresentation of the reward zone with a higher value in iHP neurons (Jin and Lee, 2021). Another recent study by Jarzebowski et al. focused on how hippocampal place cells change their firing patterns during the learning process for several sets of changing reward locations (Jarzebowski et al., 2022). The results from this study suggest that, in the iHP, the same place cells persistently fire across different reward locations, thus tracking the changes in reward locations.

Anatomically, the iHP is in an ideal position to represent associations between a

space and its value by intrahippocampal connections from both the dHP and vHP (Tao et al., 2021; Swanson et al., 1978). Importantly, the vHP is known to receive much heavier projections from value-processing subcortical areas, such as the amygdala and VTA, compared with the upper two-thirds of the hippocampus (Krettek and Price, 1977; Swanson et al., 1978; Pikkarainen et al., 1999; Felix-Ortiz and Tye, 2014; Gasbarri et al., 1994). Thus, although the iHP also receives afferent projections from these areas, it is highly likely that the vHP plays a crucial role in the value-related representation of the iHP. Notably, both the amygdala and VTA are known to be involved in processing palatability information (Tye and Janak, 2007; Fontanini et al., 2009; Chen et al., 2020), and the amygdala has a subpopulation of neurons dedicated to encoding positive values (Kim et al., 2016; Beyeler et al., 2016). These anatomical studies support our working model of the iHP in integrating place-value information.

It is worth noting that the iHP sends direct projections to the mPFC, which is thought to be involved in behavioral control and action (Hoover and Vertes, 2007; Liu and Carter, 2018). Our experimental paradigm required rats to choose and navigate towards one of two reward zones with different values, a task structure that must demand active cognitive control, presumably by the mPFC in collaboration with the hippocampus. It is also possible that inactivation of the iHP prevents the transfer of the dHP's spatial information to the mPFC via the iHP, which may explain why iHP inactivation produces severe deficits in goal-directed navigation in the current task. Based on these findings, we propose a working model in which the iHP associates spatial value information with the cognitive map of the dHP and sends value-associated spatial information to the mPFC, which translates the space-value–integrated representation into action (Bast, 2011; Bast et al., 2009).

Methods

Subjects

Eight male Long-Evans rats (8 weeks old) were housed individually under a 12-hour light/dark cycle in a temperature- and humidity-controlled environment. Rats were food-restricted to maintain ~80% of their free-feeding weight, but water was provided ad libitum. The experimental protocol (SNU-200504-3-1) complied with the guidelines of the Institutional Animal Care and Use Committee of Seoul National University.

2D VR system

We established our own VR environment consisting of a circular arena surrounded by multiple landmarks using a game engine (Unreal Engine [UE] 4.14.3; Epic Games, Inc., USA) (**Figure 1A** and **1B**). The VR environment was presented via five adjacent LCD monitors covering 270 degrees of the visual field. Rats were body-restrained at the top of a spherical treadmill, and a silicone-coated Styrofoam ball was placed on multiple ball bearings. Rats could move their heads freely; body jackets were used to anchor their positions, limiting their body movements to a 120-degree range. As rats rolled the treadmill, their movement was recorded by three rotary encoders attached to the treadmill surface. The signal from the encoders was then sent to the computer and synchronized with the movement in the virtual environment via an Arduino interface board. A licking port was placed in front of the rats and moved in association with their body movement. It was maintained in a retracted position but was extended toward the snout by a linear motor; an infrared sensor detected rats' tongues to record licking behavior. When rats arrived at either reward zone, the solenoid valve, controlled by the UE via the Arduino interface, dispensed honey water as a reward. The amount of honey water dispensed for high-value and low-value zones was maintained at a ratio (in drops) of 12:2, with 12 μL per drop.

Behavioral paradigm

After several days of handling, rats were moved to the VR apparatus and trained to roll the treadmill to navigate the virtual environment (‘Shaping’; **Figure 4B**). In this session, rats had to reach a flickering checkerboard-shaped sphere randomly spawned on a circular arena (~1.6 meters in diameter) to obtain a honeywater reward. After rats had completed more than 60 trials on two consecutive days, they were assumed to have adapted to navigating freely. They were moved to pre-surgical training (‘Pre-training’) – a 2D VR version of the place-preference task. For the pre-training session, rats were required to find hidden reward zones using the surrounding scene, including various landmarks, such as houses, mountains, and arches. The start position was located at a fixed point in the center of the arena, and reward zones were located at the east and west sides of the circular platform; reward zones were positioned at a slight distance from the arena wall to prevent rats from employing a thigmotaxis strategy. A trial started with a heading in one of six start directions, pseudorandomly chosen, and ended when the rat arrived at either reward zone. Pre-surgical training criteria were defined by the number of trials (60 trials in 40 minutes), high-value zone visit percentage (>75%), and average excess travel distance (<0.6 meters). If a rat successfully achieved training criteria 2 days in a row, it received cannula implantation surgery.

After the surgery, rats were allowed 1 week of recovery (‘Recovery’) and then were moved to post-surgical training (‘Post-training’). During post-training, rats were tested on the same place-preference task until they achieved the same criteria as pre-surgical training, except that the trial number was reduced to 40 and the average excess travel distance was reduced to less than 1 meter. This point marked the beginning of the drug injection stage; four rats received their initial injection in the dHP, and the other four rats were injected first in the iHP to counterbalance the injection order (‘Place Preference Task’).

Object-guided navigation task

After completing drug injections, we trained five of the eight rats from the main task for an object-guided navigation task to investigate whether drug infusion caused any motor- or motivation-related impairments (‘Probe’; **Figure 4B**). In this task, the rat simply had to find and navigate toward a flickering object; because there was no need for the rat to use the

646 surrounding scene to locate the reward, this probe test was hippocampus-independent. For the
647 probe test, the rat started from the south of the arena; concurrently, a flickering checkerboard-
648 shaped sphere appeared on either the left or right side of the screen. When the rat arrived at
649 the reward zone (i.e., a 0.4m-radius circle surrounding the object), the visual stimulus
650 stopped, a honeywater reward was given, and the trial ended. No landmarks surrounded the
651 circular arena to distinguish the environment from that in the main task. The criterion for
652 training included the completion of 40 trials with less than 0.1 meter of mean excess travel
653 distance, calculated as the shortest path length between the start location and the reward zone;
654 a time limit of 60 seconds was also imposed. The drug infusion schedule from the place-
655 preference task was then repeated, at which point rats were sacrificed for histological
656 procedures.

657

658 ***Surgery***

659 After rats reached pre-surgical training criteria, they were implanted with four commercial
660 cannulae (P1 Technologies, USA), bilaterally targeting the dHP and the iHP, enabling within-
661 subject comparisons in performance between dHP inactivation (dMUS) and iHP inactivation
662 (iMUS) conditions (**Figure 4A**). Animals were first anesthetized with an intraperitoneal
663 injection of sodium pentobarbital (Nembutal, 65 mg/kg), then their heads were fixed in a
664 stereotaxic frame (Kopf Instruments, USA). Isoflurane (0.5-2% mixed with 100% oxygen)
665 was used to maintain anesthesia throughout the surgery. The cannula tips targeted
666 approximately the upper blades of the dentate gyrus of both regions (AP -3.8 mm, ML ±2.6
667 mm, DV -2.7 mm for the dHP; AP -6.0 mm, ML ±5.6 mm, DV -3.2 mm with a 10-degree tilt
668 for the iHP) to inactivate each subregion effectively. The cannula, consisting of a 26-gauge
669 guide cannula coupled with a 33-gauge dummy cannula, was fixed to the target location by
670 several skull screws and bone cement. After the surgery, ibuprofen syrup was orally
671 administered for pain relief, and the animal was kept in an intensive care unit overnight.

672

673 ***Drug infusion***

674 For drug injection, the rat was first anesthetized with isoflurane. Then, 0.3 to 0.5 μl of either

675 phosphate-buffered saline (PBS) or muscimol (MUS) was infused into each hemisphere via a
676 33-gauge injection cannula at an injection speed of 0.167 μl/min. The injection cannula was
677 left in place for 1 minute after completing the drug infusion to ensure stable diffusion of the
678 drug. Then, it was slowly removed from the guide cannula and replaced by the dummy
679 cannula. The rat was kept in a clean cage for 20 minutes to recover from anesthesia
680 completely, then was moved to the VR apparatus for behavioral testing.

681

682 ***Histology***

683 After completing the probe test, animals were sacrificed by inhalation of an overdose of CO_2.
684 Rats were then transcardially perfused, first with PBS, administered with a syringe, and then
685 with a 4% v/v formaldehyde solution, delivered using a commercial pump (Masterflex Easy-
686 Load II Pump; Cole-Parmer, USA). The brain was extracted and placed in a 4% v/v
687 formaldehyde-30% sucrose solution at 4℃ until it sank to the bottom of the container. After
688 gelatin embedding, the brain was sectioned at 40 μm using a microtome (HM430; Thermo-
689 Fisher Scientific, USA), and sections were mounted on subbed slide glasses for Nissl
690 staining.

691

692 ***Statistical analysis***

693 Data were statistically analyzed using custom programs written in MATLAB R2021a
694 (MathWorks, USA), Prism 9 (GraphPad, USA), and SPSS (IBM, USA). Statistical
695 significance was determined using the Wilcoxon signed-rank test and repeated-measures
696 analysis of variance (ANOVA) followed by a Bonferroni post hoc test. For directional
697 analysis, Kuiper's test and Watson-Williams test were used. However, the latter test was
698 considered inapplicable for the mean angle when the average mean vector length between
699 two samples was less than 0.45 (Berens, 2009). The significance level was set at $\alpha = 0.05$,
700 and all error bars indicate the standard error of the mean (SEM).

701

702 **Competing Interests**

The authors have no conflicts of interest to declare.

Acknowledgments

This work was supported by the National Research Foundation of Korea (2019R1A2C2088799, 2021R1A4A2001803, 2022M3E5E8017723), BK21 FOUR program (A0462-20210100), and the Global Ph.D. Fellowship program (2019H1A2A1073456). We thank Heesoo Oh for his assistance in behavioral training.

Data Availability

The data used in this study are deposited on GitHub at https://github.com/hhwang28/Behavioral-Data.

714 ## References

715

716 Acharya L, Aghajan ZM, Vuong C, Moore JJ, Mehta MR (2016) **Causal influence of visual**
717 **cues on hippocampal directional selectivity** *Cell* **164**: 197–207.
718 Aronov D, Tank DW (2014) **Engagement of neural circuits underlying 2D spatial**
719 **navigation in a rodent virtual reality system** *Neuron* **84**: 442–456.
720 Bast T (2011) **The hippocampal learning-behavior translation and the functional**
721 **significance of hippocampal dysfunction in schizophrenia** *Current Opinion in*
722 *Neurobiology* **21**: 492–501.
723 Bast T, Wilson IA, Witter MP, Morris RGM (2009) **From rapid place learning to**
724 **behavioral performance: A key role for the intermediate hippocampus** *PLoS Biology*
725 **7**: e1000089.
726 Berens P (2009) **CircStat: A MATLAB toolbox for circular statistics** *Journal of Statistical*
727 *Software* **31**: 1–21.
728 Beyeler A, Namburi P, Glober GF, Simonnet C, Calhoon GG, Conyers GF, Luck R, Wildes
729 CP, Tye KM (2016) **Divergent routing of positive and negative information from the**
730 **amygdala during memory retrieval** *Neuron* **90**: 348–361.
731 Biane JS, Ladow MA, Stefanini F, Boddu SP, Fan A, Hassan S, Dundar N, Apodaca-
732 Montano DL, Zhou LZ, Fayner V, Woods NI, Kheirbek MA (2023) **Neural dynamics**
733 **underlying associative learning in the dorsal and ventral hippocampus** *Nature*
734 *Neuroscience* **26**: 798–809.
735 Bienkowski MS, Bowman I, Song MY, Gou L, Ard T, Cotter K, Zhu M, Benavidez NL,
736 Yamashita S, Abu-Jaber J, Azam S, Lo D, Foster NN, Hintiryan H, Dong H-W (2018)
737 **Integration of gene expression and brain-wide connectivity reveals the multiscale**
738 **organization of mouse hippocampal networks** *Nature Neuroscience* **21**: 1628–1643.
739 Chen L, Lu Y-P, Chen H-Y, Huang S-N, Guo Y-R, Zhang J-Y, Li Q-X, Luo C-Y, Lin S-W,
740 Chen Z-N, Hu L-H, Wang W-X, Li H-Y, Cai P, Yu C-X (2020) **Ventral tegmental area**
741 **GABAergic neurons induce anxiety-like behaviors and promote palatable food**
742 **intake** *Neuropharmacology* **173**: 108114.

De Hoz L, Knox J, Morris RGM (2003) **Longitudinal axis of the hippocampus: Both septal and temporal poles of the hippocampus support water maze spatial learning depending on the training protocol** *Hippocampus* **13**: 587–603.

Dolorfo CL, Amaral DG (1998) **Entorhinal cortex of the rat: Organization of intrinsic connections** *Journal of Comparative Neurology* **398**: 49-82.

Dong H-W, Swanson LW, Chen L, Fanselow MS, Toga AW (2009) **Genomic–anatomic evidence for distinct functional domains in hippocampal field CA1** *Proceedings of the National Academy of Sciences* **106**: 11794–11799.

Dupret D, O'Neill J, Pleydell-Bouverie B, Csicsvari J (2010) **The reorganization and reactivation of hippocampal maps predict spatial memory performance** *Nature Neuroscience* **13**: 995–1002.

Duvelle É, Grieves RM, Hok V, Poucet B, Arleo A, Jeffery K, Save E (2019) **Insensitivity of place cells to the value of spatial goals in a two-choice flexible navigation task** *The Journal of Neuroscience* **39**: 2522-2541.

Felix-Ortiz AC and Tye KM (2014) **Amygdala inputs to the ventral hippocampus bidirectionally modulate social behavior** *The Journal of Neuroscience* **34**: 586-595.

Fontanini A, Grossman SE, Figueroa JA, Katz DB (2009) **Distinct subtypes of basolateral amygdala taste neurons reflect palatability and reward** *The Journal of Neuroscience*, **29**: 2486–2495.

Gasbarri A, Packard MG, Campana E, Pacitti C (1994) **Anterograde and retrograde tracing of projections from the ventral tegmental area to the hippocampal formation in the rat** *Brain Research Bulletin* **33**: 445–452.

Gauthier JL, Tank DW (2018) **A dedicated population for reward coding in the hippocampus** *Neuron* **99**: 179-193.e7.

Georges-Francois P, Rolls ET, Robertson RG (1999) **Spatial view cells in the primate hippocampus: Allocentric view not head direction or eye position or place** *Cerebral Cortex* **9**: 197–212.

Gothard K, Skaggs W, Moore K, McNaughton B (1996) **Binding of hippocampal CA1 neural activity to multiple reference frames in a landmark-based navigation task** *The Journal of Neuroscience* **16**: 823–835.

773 Hollup SA, Molden S, Donnett JG, Moser M-B, Moser EI (2001) **Accumulation of**
774 **hippocampal place fields at the goal location in an annular watermaze task** *The*
775 *Journal of Neuroscience* **21**: 1635–1644.
776 Hoover WB, Vertes RP (2007) **Anatomical analysis of afferent projections to the medial**
777 **prefrontal cortex in the rat** *Brain Structure and Function* **212**: 149–179.
778 Jarzebowski P, Hay YA, Grewe BF, Paulsen O (2022) **Different encoding of reward**
779 **location in dorsal and intermediate hippocampus** *Current Biology* **32**: 834-841.e5.
780 Jin S-W, Lee I (2021) **Differential encoding of place value between the dorsal and**
781 **intermediate hippocampus** *Current Biology* **31**: 3053-3072.e5.
782 Jung M, Wiener S, McNaughton B (1994) **Comparison of spatial firing characteristics of**
783 **units in dorsal and ventral hippocampus of the rat** *The Journal of Neuroscience*, **14**:
784 7347–7356.
785 Kennedy PJ, Shapiro ML (2009) **Motivational states activate distinct hippocampal**
786 **representations to guide goal-directed behaviors** *Proceedings of the National*
787 *Academy of Sciences* **106**: 10805–10810.
788 Kim J, Pignatelli M, Xu S, Itohara S, Tonegawa S (2016) **Antagonistic negative and**
789 **positive neurons of the basolateral amygdala** *Nature Neuroscience* **19**: 1636–1646.
790 Kjelstrup KB, Solstad T, Brun VH, Hafting T, Leutgeb S, Witter MP, Moser EI, Moser M-B
791 (2008) **Finite scale of spatial representation in the hippocampus** *Science* **321**: 140–
792 143.
793 Krettek JE, Price JL (1977) **Projections from the amygdaloid complex and adjacent**
794 **olfactory structures to the entorhinal cortex and to the subiculum in the rat and cat**
795 *Journal of Comparative Neurology* **172**: 723–752.
796 Lee I, Griffin AL, Zilli EA, Eichenbaum H, Hasselmo ME (2006) **Gradual translocation of**
797 **spatial correlates of neuronal firing in the hippocampus toward prospective reward**
798 **locations** *Neuron* **51**: 639–650.
799 Liu X, Carter AG (2018) **Ventral hippocampal inputs preferentially drive corticocortical**
800 **neurons in the infralimbic prefrontal cortex** *The Journal of Neuroscience* **38**: 7351–
801 7363.

Markus E, Qin Y, Leonard B, Skaggs W, McNaughton B, Barnes C (1995) **Interactions between location and task affect the spatial and directional firing of hippocampal neurons** *The Journal of Neuroscience* **15**: 7079–7094.

Morris RGM, Hagan JJ, Rawlins JNP (1986) **Allocentric spatial learning by hippocampectomised rats: A further test of the "spatial mapping" and "working memory" theories of hippocampal function** *The Quarterly Journal of Experimental Psychology* **38**: 365-395.

Moser MB, Moser EI, Forrest E, Andersen P, Morris RG (1995) **Spatial learning with a minislab in the dorsal hippocampus** *Proceedings of the National Academy of Sciences* **92**: 9697–9701.

O'Keefe J, Dostrovsky J (1971) **The hippocampus as a spatial map. Preliminary evidence from unit activity in the freely-moving rat** *Brain Research* **34**: 171–175.

O'Keefe J, Nadel L (1978) *The hippocampus as a cognitive map*. Oxford: Clarendon.

Packard MG, Hirsh R, White NM (1989) **Differential effects of fornix and caudate nucleus lesions on two radial maze tasks: evidence for multiple memory systems** *The Journal of Neuroscience* **9**: 1465-1472.

Pikkarainen M, Rönkkö S, Savander V, Insausti R, Pitkänen A (1999) **Projections from the lateral, basal, and accessory basal nuclei of the amygdala to the hippocampal formation in rat** *Journal of Comparative Neurology* **403**: 229–260.

Ravassard P, Kees A, Willers B, Ho D, Aharoni D, Cushman J, Aghajan ZM, Mehta MR (2013) **Multisensory control of hippocampal spatiotemporal selectivity** *Science* **340**: 1342–1346.

Rolls ET, O'Mara SM (1995) **View-responsive neurons in the primate hippocampal complex** *Hippocampus* **5**: 409–424.

Royer S, Sirota A, Patel J, Buzsaki G (2010) **Distinct representations and theta dynamics in dorsal and ventral hippocampus** *The Journal of Neuroscience* **30**: 1777–1787.

Speakman A, O'Keefe J (1990) **Hippocampal complex spike cells do not change their place fields if the goal is moved within a cue controlled environment** *European Journal of Neuroscience* **2**: 544–555.

Swanson LW, Wyss JM, Cowan WM (1978) **An autoradiographic study of the organization of intrahippocampal association pathways in the rat** *Journal of Comparative Neurology* **181**: 681–715.

Tao S, Wang Y, Peng J, Zhao Y, He X, Yu X, Liu Q, Jin S, Xu F (2021) **Whole-brain mapping the direct inputs of dorsal and ventral CA1 projection neurons** *Frontiers in Neural Circuits* **15**: 643230.

Tye KM, Janak PH (2007) **Amygdala neurons differentially encode motivation and reinforcement** *The Journal of Neuroscience* **27**: 3937–3945.

Valenti O, Mikus N, Klausberger T (2018) **The cognitive nuances of surprising events: Exposure to unexpected stimuli elicits firing variations in neurons of the dorsal CA1 hippocampus** *Brain Structure and Function* **223**: 3183–3211.

Van Groen T, Wyss JM (2003) **Connections of the retrosplenial granular b cortex in the rat** *Journal of Comparative Neurology* **463**: 249-263.

Figure Legends

Figure 1. Place-preference task in a 2D VR environment. (A) 2D VR setup. (B) Bird's-eye view of the virtual environment. Various landmarks surrounded a circular arena, and a fixed start location ('St') was at the center. Reward zones are illustrated with white dashed lines for visualization purposes. (C) Place-preference task paradigm. A trial started with one of six pseudorandomly chosen start directions ('Trial Start'). In this example, the rat started the trial facing the northeast (NE) direction, highlighted in green. Subsequent navigation is illustrated here with the associated scene ('Navigation'). A dot on the gray trajectory indicates the rat's current location and the black arrow describes the head direction. When the rat arrived at a reward zone, honey water was delivered within 8 seconds, with the visual scene frozen ('Reward'). Finally, a gray screen appeared, denoting an inter-trial interval; if the rat remained still (<5 cm/s) for 5 seconds, the subsequent trial began ('ITI').

Figure 2. Common body-turning behavior of rats after learning. (A) The reference frame of the virtual environment. The six start directions are illustrated with the red high-value zone (180°) and blue low-value zone (0°). On the right, the departure circle (DC) is denoted with a purple dashed line, and the start direction is marked with a black arrowhead and a green arrow. (B) Overall changes in scene direction over the normalized distance between the start location and the DC (left). Each colored line indicates the median change of scene direction in trials with each start location, and red and blue arrowheads mark high- and low-value zone centers, respectively. The 0°-to-360° range was repeated in the ordinate of the plot to capture rotational movements in opposite directions (positive and negative directions for clockwise and counterclockwise rotations, respectively). The gray lines on the right show the rat's trajectory within the DC. These examples were excerpted from the first and last days of pre-training of a single rat. (C) Individual examples of scene directions and trajectories in the novice session. Scene direction change for each direction is drawn separately (top) for individual trials. The black arrowhead indicates that specific start direction. Trajectories within the DC (middle) and the whole arena (bottom) are also illustrated according to the indicated color code. Mean travel distance and latency are shown below the VR arena trajectory. (D) Same as (C), but for the expert session.

Figure 3. Learning index for efficient navigation during pre-surgical training. (A) Changes in departing direction (DD) with learning. (i) Schematic of DD (purple dot), with the departure circle shown as a dashed line. (ii) Distribution of DDs in pre- and post-learning sessions from all rats (rose plots). Gray denotes the pre-learning session, whereas purple indicates the post-learning session. Mean vectors are illustrated as arrows with the same color scheme, and their lengths are indicated at the upper right side of the plot. (iii) Schematic of the DD-deviation angle (angle between the high-value zone center and the DD) and comparisons of DD-deviation angles between pre- and post-learning sessions. Each dot represents data from one rat. (B) Same as (A), but for perimeter-crossing direction (PCD; green dot). The perimeter is drawn as a green dashed circle. **$p < 0.01$.

Figure 4. Cannula implantation locations and schedules for training and drug injection. (A) Cannula positions marked. (i) Example of bilaterally implanted cannula tracks in Nissl-stained sections in the dHP and iHP. (ii) Tip locations illustrated in the atlas, with different colors for individual rats (n = 8). (B) Training schedule. Rats were divided into two groups (n = 4/group) to counterbalance the injection order for the main task and probe test.

Figure 5. Changes in navigational pattern with each drug condition. (A) Sample trajectories in each drug condition. Black arrowheads indicate the start direction and the gray line shows the trajectory for each trial. (B) Mean high-value zone visit percentage for each drug condition. Gray, green, and orange each indicate PBS, dMUS, and iMUS sessions, respectively. (C) Average running speed. (D) Number of perimeter crossings. For the PBS session, dPBS and iPBS sessions were first tested for significant differences between sessions; if they were not different, they were averaged to one PBS session for analysis purposes. *$p < 0.05$.

Figure 6. dHP and iHP inactivation differentially affect efficient goal-directed navigation. (A) Grouped comparison of DD in each drug condition. (i) Distributions of DDs in each drug condition (rose plots) and a comparison of their mean directions. Gray plots, PBS sessions;

green plots, dHP inactivation; orange plots, iHP inactivation. Red and blue arcs indicate high- and low-value zones, respectively. Statistically significant differences in mean vectors, illustrated as arrows, are indicated with asterisks. The mean directions of all four conditions were first compared together (Watson-Williams test); a post hoc pairwise comparison was subsequently applied if the average mean vector length of the two sessions was greater than 0.45. The number on the upper right side of the plot shows the length of the mean vector. (B, C) Changes in mean vector length (B) and deviation angles from the high-value zone center (C) of the DD in each drug session. *$p < 0.05$, **$p < 0.01$, ***$p < 0.001$.

Figure 7. Accuracy of goal-directed navigation is more severely impaired with iHP inactivation. (A-C) Same as Figure 6, except showing PCD. *$p < 0.05$, **$p < 0.01$, ***$p < 0.001$.

Figure 8. Goal-directedness and navigational capacity are unaffected by drug infusion. (A) Object-guided navigation task as a probe test. (i) A flickering object appeared on either the left ('Left trial') or right ('Right trial') side of the screen. The start location is marked with a yellow dot, with a white arrow indicating the start direction, which remained the same for both trial types. (ii) Example of trajectories in one session. Blue and red lines represent trajectories from left and right trials that directly arrived at the reward zones, whereas gray lines indicate failed trials. Green dashed lines denote reward zones. (B) Comparison of the proportion of each drug condition's direct hit trials (both left and right).

Figure 1

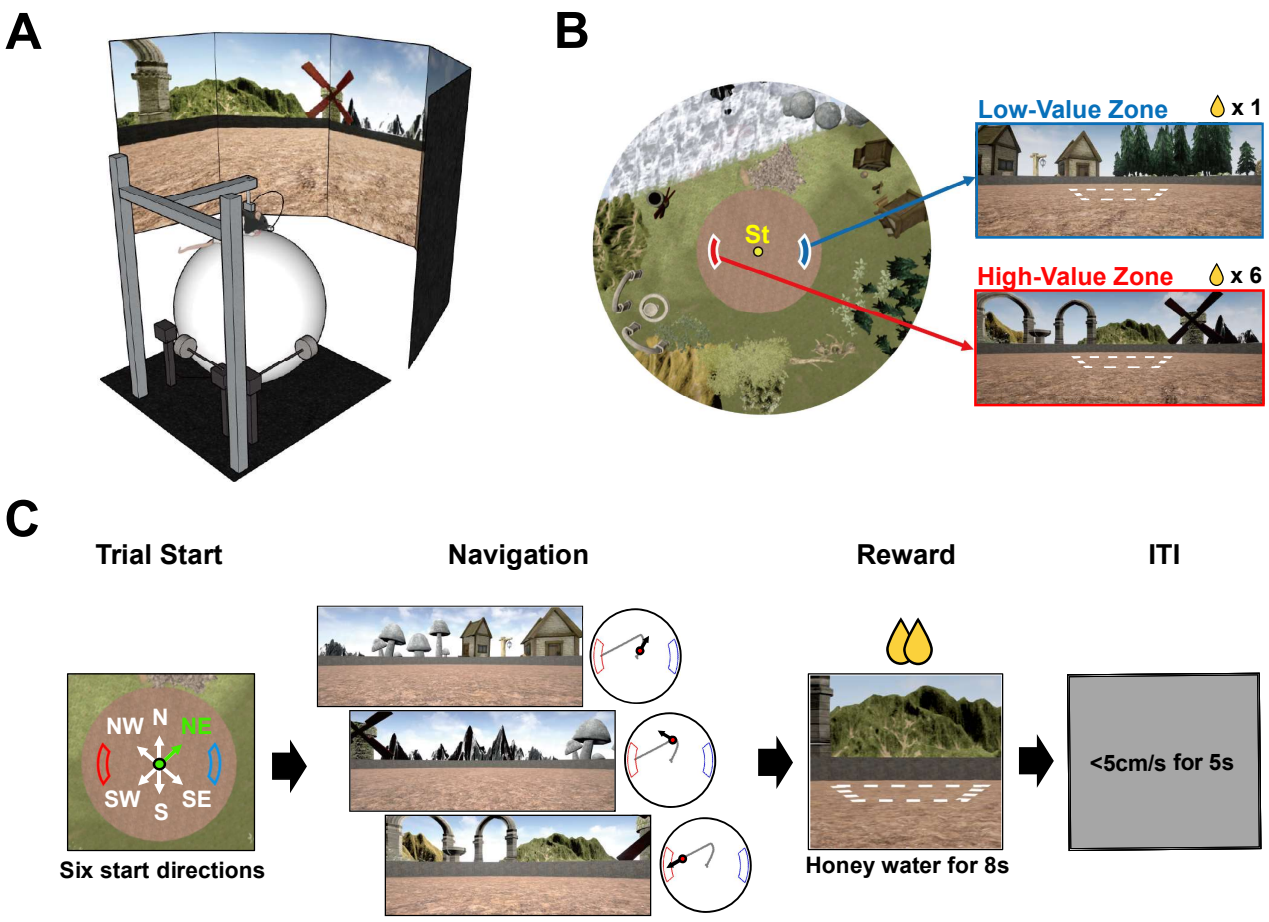
A
B
St
Low-Value Zone
x 1
High-Value Zone
x 6
C
Trial Start
Navigation
Reward
ITI
NW
N
NE
SW
S
SE
Six start directions
Honey water for 8s
<5cm/s for 5s

Figure 2

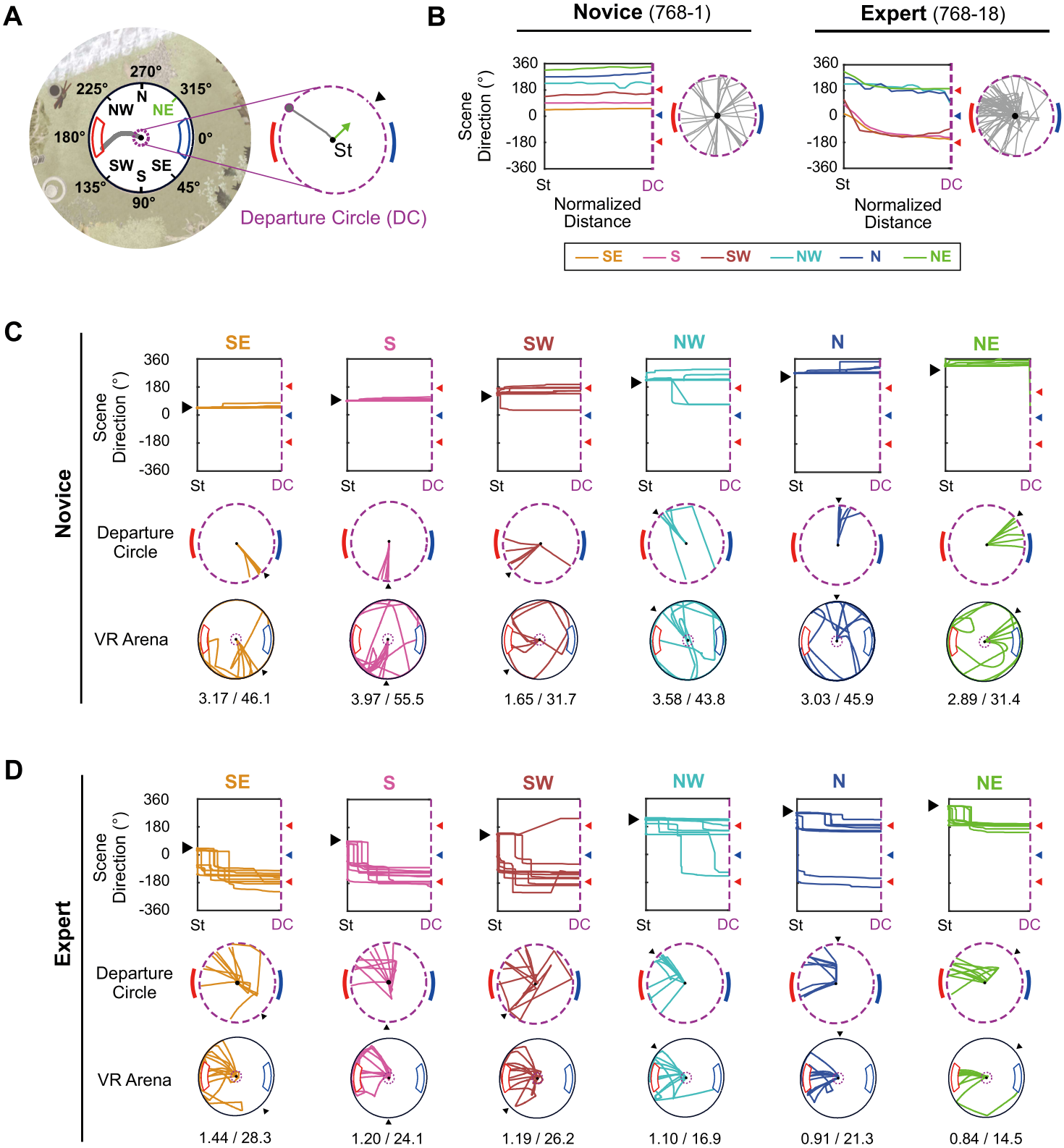
A
270°
225°
315°
N
NW
NE
180°
0°
SW
SE
S
135°
45°
90°
St
Departure Circle (DC)
B
Novice (768-1)
Expert (768-18)
Scene Direction (°)
360
180
0
-180
-360
St
DC
Normalized Distance
SE
S
SW
NW
N
NE
C
Novice
SE
S
SW
NW
N
NE
Scene Direction (°)
Departure Circle
VR Arena
3.17 / 46.1
3.97 / 55.5
1.65 / 31.7
3.58 / 43.8
3.03 / 45.9
2.89 / 31.4
D
Expert
1.44 / 28.3
1.20 / 24.1
1.19 / 26.2
1.10 / 16.9
0.91 / 21.3
0.84 / 14.5

Figure 3

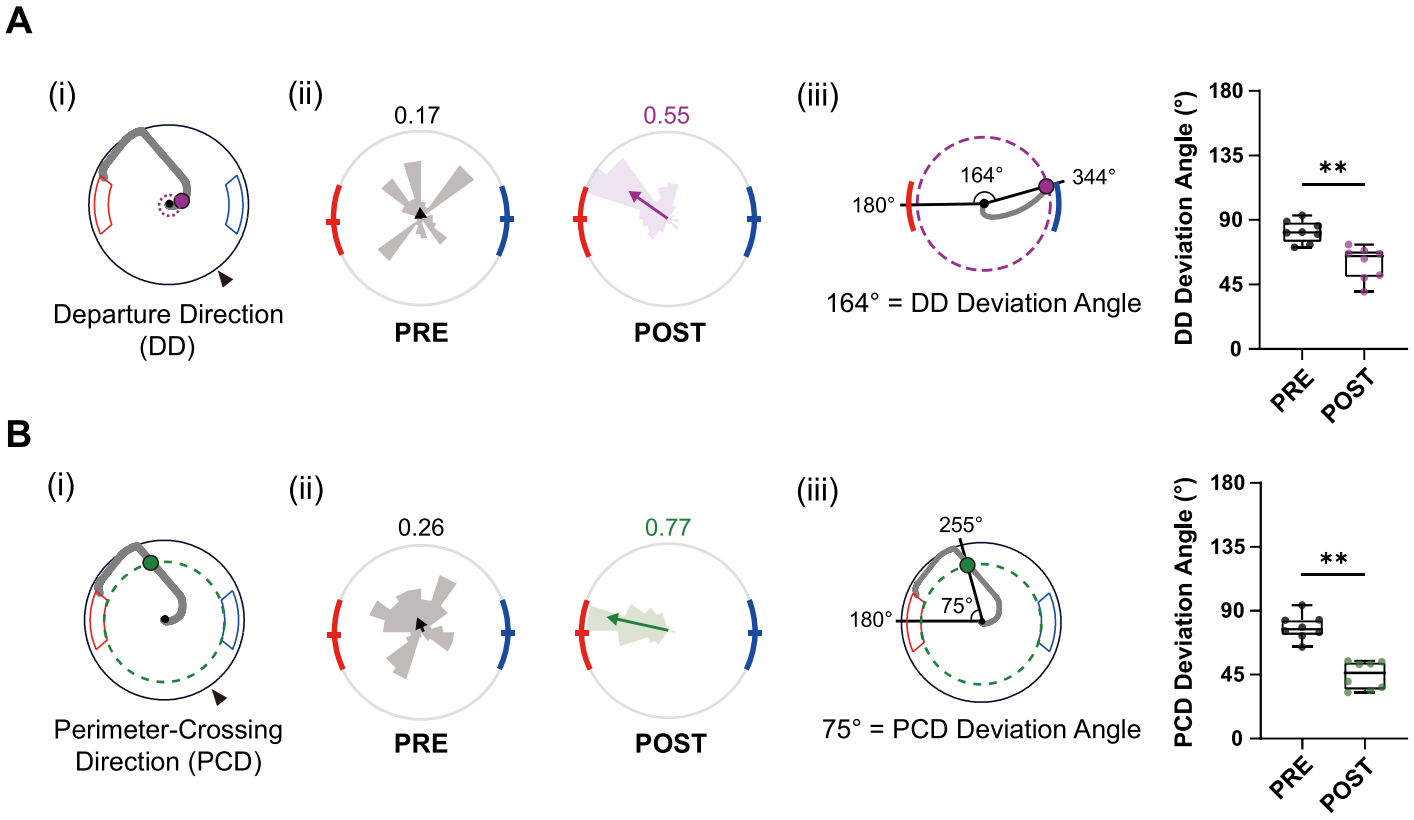
A
(i)
Departure Direction
(DD)
(ii)
0.17
PRE
0.55
POST
(iii)
180°
164°
344°
164° = DD Deviation Angle
DD Deviation Angle (°)
180
135
90
45
0
**
PRE
POST
B
(i)
Perimeter-Crossing
Direction (PCD)
(ii)
0.26
PRE
0.77
POST
(iii)
255°
180°
75°
75° = PCD Deviation Angle
PCD Deviation Angle (°)
180
135
90
45
0
**
PRE
POST

Figure 4

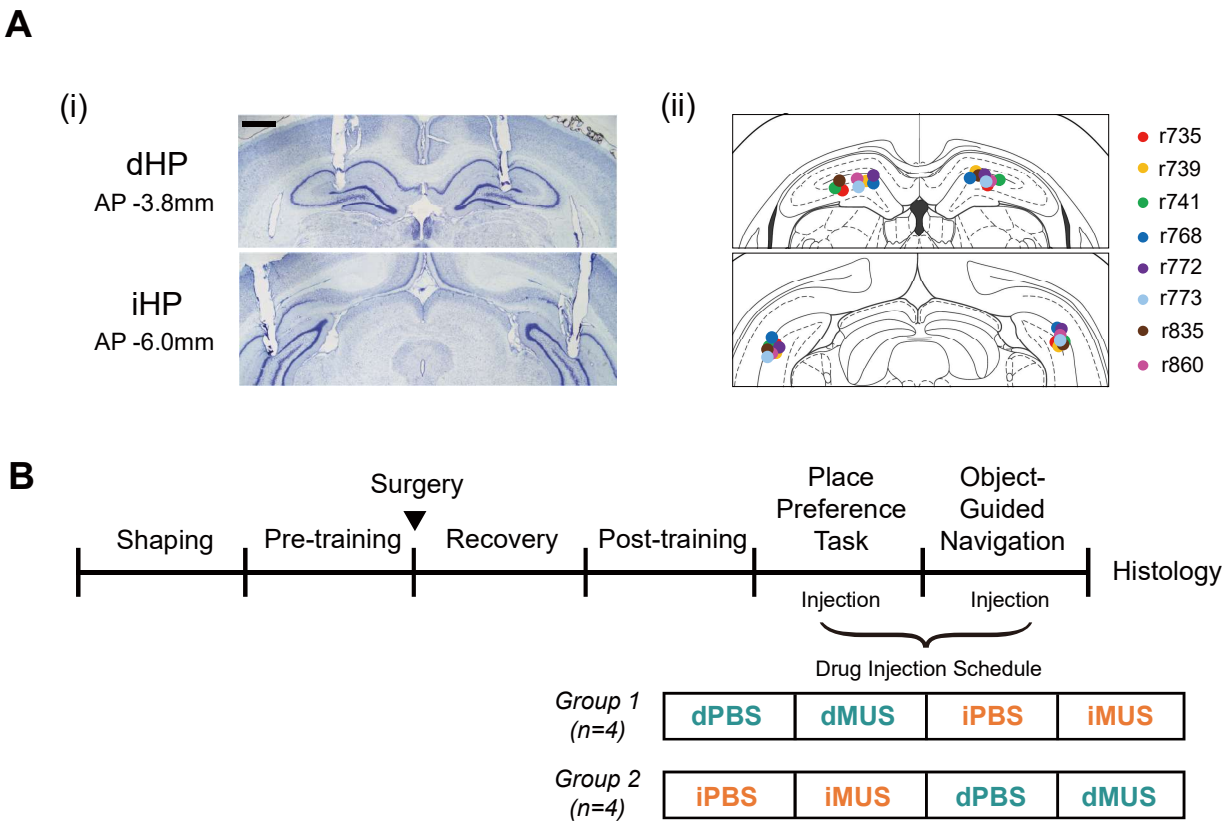
A
(i)
dHP
AP -3.8mm
iHP
AP -6.0mm
(ii)
r735
r739
r741
r768
r772
r773
r835
r860
B
Surgery
Shaping
Pre-training
Recovery
Post-training
Place Preference Task
Object-Guided Navigation
Histology
Injection
Injection
Drug Injection Schedule
Group 1 (n=4)
dPBS
dMUS
iPBS
iMUS
Group 2 (n=4)
iPBS
iMUS
dPBS
dMUS

Figure 5

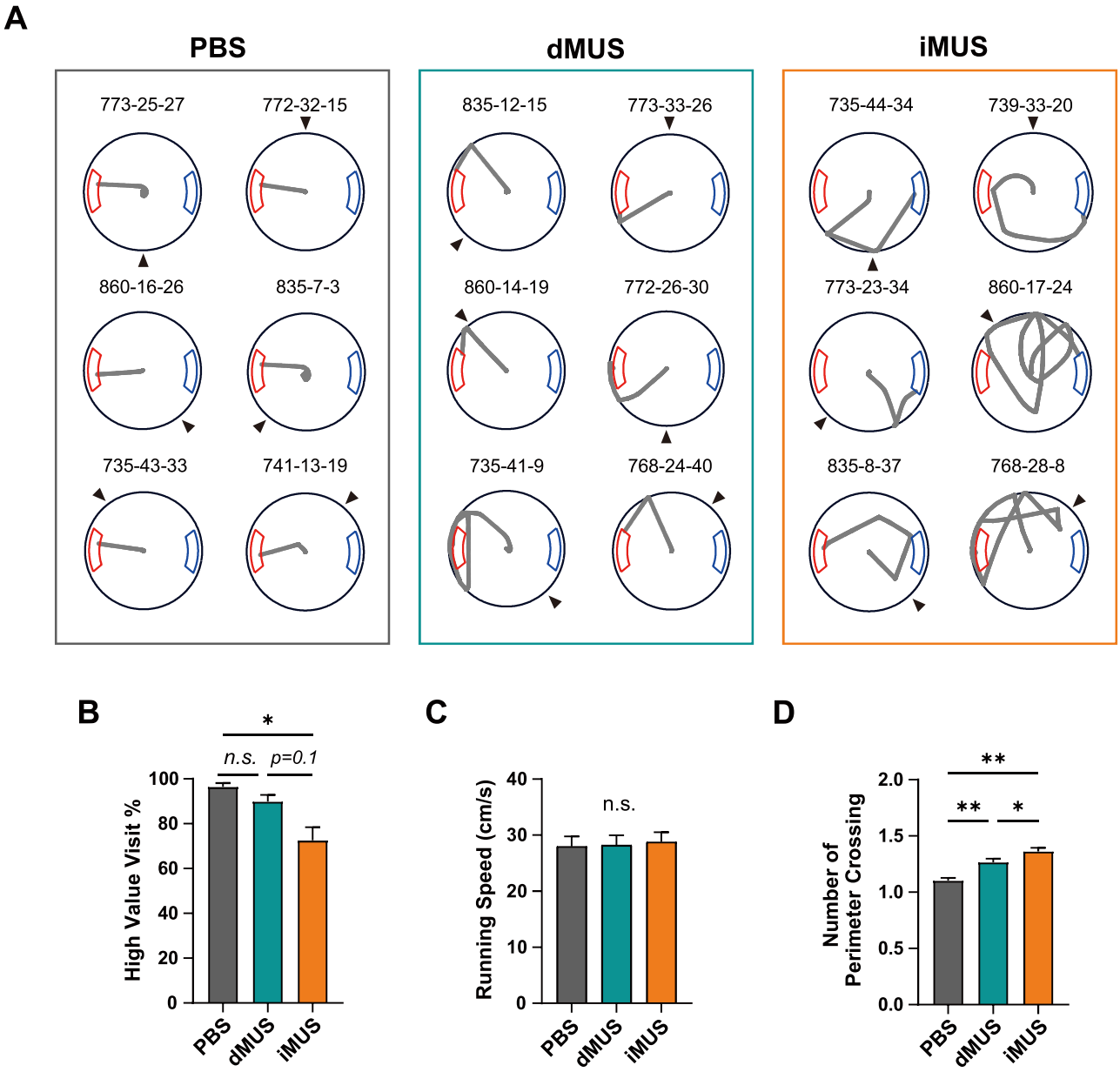
A
PBS
773-25-27
772-32-15
860-16-26
835-7-3
735-43-33
741-13-19
dMUS
835-12-15
773-33-26
860-14-19
772-26-30
735-41-9
768-24-40
iMUS
735-44-34
739-33-20
773-23-34
860-17-24
835-8-37
768-28-8
B
High Value Visit %
100
80
60
40
20
0
*
n.s.
p=0.1
PBS
dMUS
iMUS
C
Running Speed (cm/s)
40
30
20
10
0
n.s.
PBS
dMUS
iMUS
D
Number of Perimeter Crossing
2.0
1.5
1.0
0.5
0.0
**
**
*
PBS
dMUS
iMUS

Figure 6

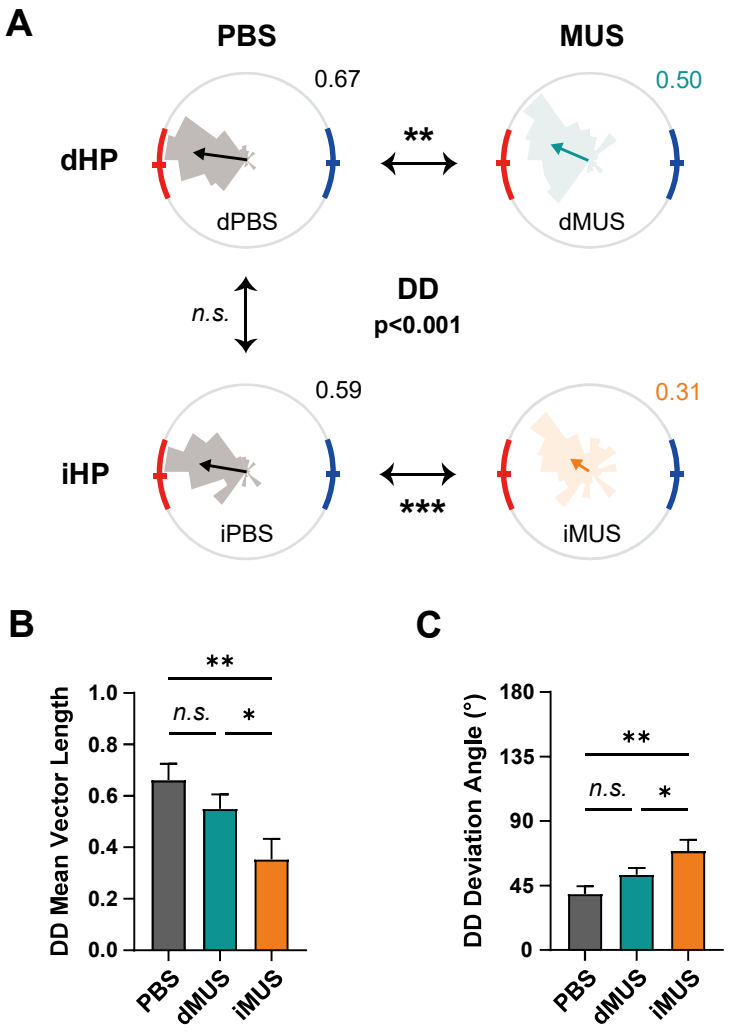
A
PBS
MUS
0.67
0.50
dHP
**
dPBS
dMUS
n.s.
DD
p<0.001
0.59
0.31
iHP
***
iPBS
iMUS
B
DD Mean Vector Length
1.0
0.8
0.6
0.4
0.2
0.0
**
n.s.
*
PBS
dMUS
iMUS
C
DD Deviation Angle (°)
180
135
90
45
0
**
n.s.
*
PBS
dMUS
iMUS

Figure 7

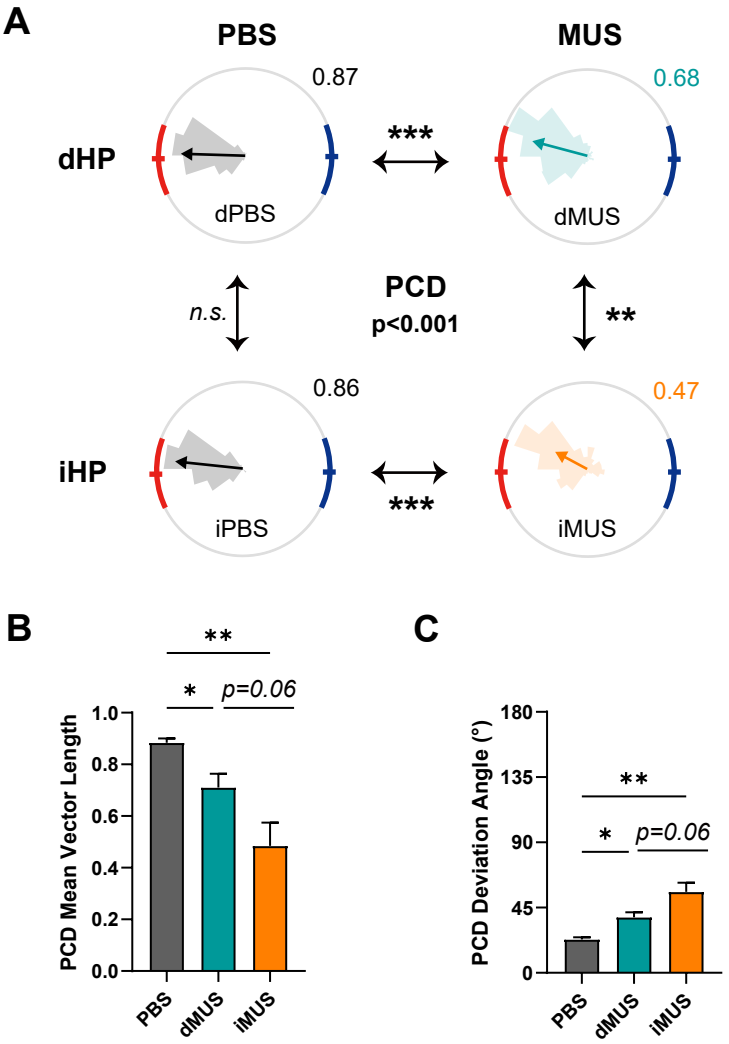
A
PBS
MUS
0.87
0.68
dHP
***
dPBS
dMUS
n.s.
PCD
p<0.001
**
0.86
0.47
iHP
***
iPBS
iMUS
B
**
*
p=0.06
PCD Mean Vector Length
1.0
0.8
0.6
0.4
0.2
0.0
PBS
dMUS
iMUS
C
PCD Deviation Angle (°)
180
135
90
45
0
**
*
p=0.06
PBS
dMUS
iMUS

Figure 8

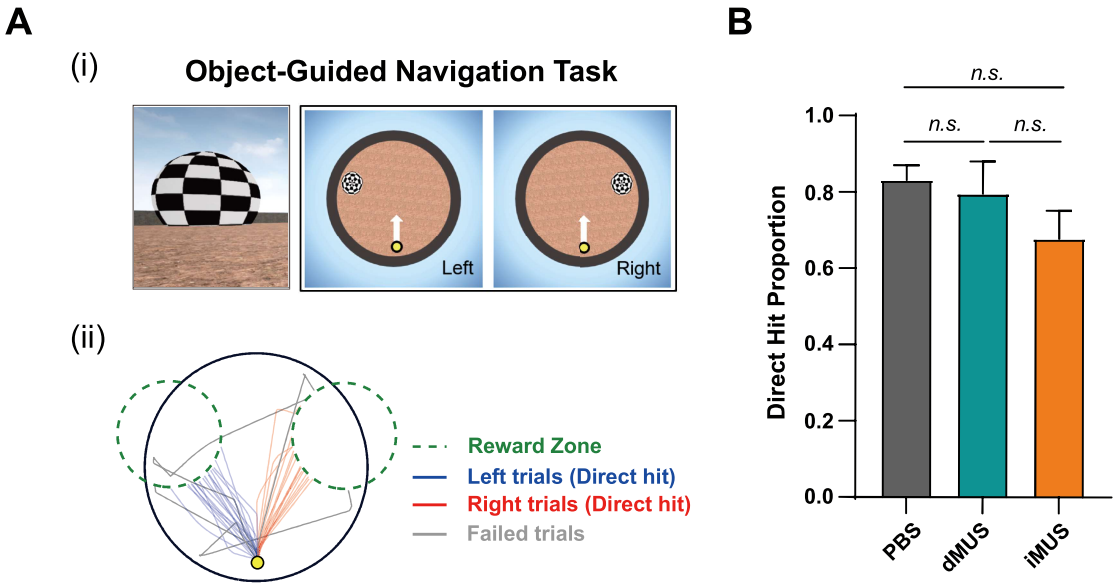
A
(i)
Object-Guided Navigation Task
Left
Right
(ii)
Reward Zone
Left trials (Direct hit)
Right trials (Direct hit)
Failed trials
B
n.s.
n.s.
n.s.
Direct Hit Proportion
1.0
0.8
0.6
0.4
0.2
0.0
PBS
dMUS
iMUS